PCCP

Tuning the surface composition of Cu3Au binary alloy

Journal:	*Physical Chemistry Chemical Physics*
Manuscript ID	CP-ART-10-2019-005729.R1
Article Type:	Paper
Date Submitted by the Author:	31-Dec-2019
Complete List of Authors:	Li, Chaoran; State University of New York at Binghamton Liu, Qianqian; State University of New York at Binghamton Bosoboinik, J. Anibal; Brookhaven National Laboratory Zhou, Guangwen; State University of New York at Binghamton

Tuning the surface composition of Cu_3Au binary alloy

Chaoran Li[1], Qianqian Liu[1], Jorge Anibal Boscoboinik[2], Guangwen Zhou[1]*

[1]Department of Mechanical Engineering & Materials Science and Engineering Program, State University of New York at Binghamton, New York 13902

[2]Center for Functional Nanomaterials, Brookhaven National Laboratory, Upton, New York 11973

Abstract

Using ambient-pressure X-ray photoelectron spectroscopy, here we report the real-time monitoring of dynamic surface composition evolution of $Cu_3Au(100)$ in response to the imposed environmental stimuli. Segregation of Au to the pristine surface under ultrahigh vacuum annealing leads to the phase separation with pure Au at the surface and alloyed Au in the subsurface. Upon switching to an oxidizing atmosphere, oxygen adsorption drives the surface segregation of Cu along with inward migration of pure Au to the subsurface. Switching to a H_2 atmosphere results in oxygen loss from the oxygenated surface, thereby promoting Au surface segregation and reverting the surface to the pristine state with the Au termination. These measurements demonstrated the tunability of the surface composition of the binary alloy by utilizing the interplay between the tendency of segregating a more noble constituent to the surface and the tendency to segregate the more reactive one with the chemical stimuli.

Correspondence should be addressed to: gzhou@binghamton.edu

1. Introduction

Although phase diagrams delineating phase/structure selection in bulk alloys in certain thermodynamic conditions are well established, the composition and structure of an alloy surface can be significantly different from those of the bulk due to surface segregation of the alloying element. This phenomenon has direct relevance to technology-related properties of alloys because the resulting minor compositional changes at the surface can lead to drastic changes in material properties ranging from the catalytic performance[1,2], corrosion resistance[3,4], kinetics of phase transformation[5,6], to the mechanical behavior[7,8]. The circumstances under which surface segregation occurs vary and the nature of the segregation depends on the specifics of the surrounding environment. It is generally believed that the element with a smaller surface energy segregates to the surface under idealized conditions[5,9–17], i.e., ultrahigh vacuum (UHV), whereas the alloy element that form stronger bonds with gas species becomes enriched at the surface in a reactive environment[5,9,10,18–25]. The interest in the surface segregation phenomena is motivated by utilizing this interplay between the tendency of segregating a more noble constituent to the surface and the tendency to segregate the more reactive one to tune the surface composition of alloys. Such fundamental knowledge has great practical importance for manipulating the properties and functionality of the alloys via exploiting the environmental bias. Until now, this level of knowledge is still very shallow for everything that goes beyond the idealized UHV conditions. Few experimental studies on tuning the surface segregation of alloys have been reported and the atomic processes governing the onset, promotion, and termination of surface segregation under practical environmental conditions are largely unknown. This lack of knowledge is largely because most surface-sensitive techniques such as Auger electron spectroscopy (AES), low energy ion scattering spectroscopy (LEIS) and X-ray photoelectron spectroscopy (XPS) for surface composition measurements are typically limited to high-vacuum environments.

Our current understanding of surface segregation under reactive conditions is therefore largely derived from “quench-and-look” studies. This is, the surface is quenched after a certain amount of reaction period, followed by an examination of the surface composition. However, dynamic changes in

the surface composition are difficult to extract with this approach and post-reaction examinations of a static surface do not often accurately represent its state in the reaction environments. Another issue for post-examination is atmospheric contamination that may bring controversies in understanding segregation mechanism. The recent development of new experimental tools with environmental capabilities makes it now possible to measure the dynamic evolution of surface composition in the presence of gases at elevated pressures. Ambient-pressure X-ray photoelectron spectroscopy (AP-XPS) is one of these tools that is capable of monitoring the chemical states and surface composition at the atomic scale and in real time with the gas pressure varying from UHV to a few Torr[26]. In this work, we describe AP-XPS measurements of the dynamic evolution of surface segregation of $Cu_3Au(100)$ in response to environmental stimuli. We consider here the binary Cu_3Au for both its fundamental and practical importance. Cu_3Au undergoes the well-known order-disorder phase transition that may have an important implication for studying the surface segregation behavior. This is because of the interplay between surface segregation and chemical ordering[6,11,27,28], where the former results in the occupation of neighboring lattice sites by the same atomic species at the surface sites whereas the latter causes exactly the opposite. Practically, the catalytic activities of Au have received a lot of attention. The chemical properties of the localized Au atoms depend on their surroundings[29,30]. A Cu_3Au surface can be a model system for establishing the fundamental principles to control the chemical properties by tuning the surface segregation.

2. Experiments

The ambient-pressure photoelectron experiments were performed at the IOS beamline of the National Synchrotron Light Source II (NSLS-II), Brookhaven National Laboratory. The AP-XPS system consists of a sample compartment (main chamber) with the base pressure $<5\times10^{-9}$ Torr, a SPECS PHOIBOS NAP 150 hemispherical analyzer, and an Ar-ion sputtering gun. The multiple differential pumping stages between the main chamber and the hemispherical analyzer result in different gas pressures in these two chambers by maintaining UHV conditions (lower than 1×10^{-7} Torr) in the analyzer

when the pressure in the main chamber is a few Torr. Photoemitted electrons leave the high-pressure sample compartment through a small aperture in a conical piece into the differentially pumped transfer lens system toward the electron energy analyzer, allowing for continuously acquiring XPS spectra at pressures of up to ~5 Torr. The photon energy range of the beamline is from 250 to 2000 eV, which covers O 1s, C 1s, Au 4f and Cu 2p core levels relevant for the current work. Real-time monitoring of the surface chemistry and composition evolution was performed by acquiring XPS spectra in situ in the presence of gas. Identification of the surface sensitivity of each species in the near-surface region was performed using depth profiling of the chemical composition by variation of the incident photon energy from 400 eV to 1250 eV. All spectra were collected at the takeoff angle of 20° between the sample surface and the electron analyzer optics of the XPS spectrometer. Binding energies in each spectrum were corrected by referring to the Fermi level and to metallic Au $4f_{7/2}$ at the binding energy of 84.0 eV. XPS spectra were analyzed using a Shirley-type background with the Voigt function. Line shape of a Gaussian/Lorentzian sum formula modified by the exponential blend was introduced for accurate peak fitting and deconvolution. Full width at half-maximum (FWHM) of Au is 0.5-0.6 eV for alloyed Au and 0.4-0.5 eV for metallic Au. Integrated peak areas of each Au species were used to calculate the relative composition evolution.

The $Cu_3Au(100)$ single crystal (Princeton Scientific Corp, purity = 99.9999%) is a top-hat-shaped disc (1 mm thick and 8 mm in diameter), cut to within 0.1° to the (100) crystallographic orientation and polished to a mirror finish. The crystal was heated via a ceramic button heater and its temperature was monitored with a type-K thermocouple. The pristine $Cu_3Au(100)$ crystal was cleaned by repeated cycles of Ar-ion$^+$ bombardment (5×10^{-5} Torr of Ar, 1 μA cm^{-2}, 1.0 keV, 20 min) at room temperature followed by UHV annealing (550°C, 10 min) until no O 1s and C 1s spectra could be detected using XPS. A separate system equipped with the capabilities for surface structure determination, that is, low-energy electron diffraction and scanning tunneling microscopy, was used to check the surface quality of the $Cu_3Au(100)$ prepared using the same sputtering and annealing procedure as the AP-XPS experiments. The as-cleaned surface appeared as flat terraces separated by atomic height steps and showed sharp

diffraction spots of the c(2×2) reconstruction, confirming that the surface at room temperature practically preserved the chemical ordering of the ideal bulk termination with outermost layers alternating between mixed $Cu_{0.5}Au_{0.5}$ and pure Cu, consistent with previous studies[31,32]. High-purity oxygen and hydrogen gases (purity = 99.9999%) were directly introduced to the sample compartment through separate variable-pressure leak valves to tune the surface segregation of either Cu or Au atoms.

3. Results

3.1 Segregation of the pristine surface under ultrahigh vacuum condition

Cu_3Au is a classic ordering alloy with the bulk order-disorder phase transition at T = 390°C. We measure the surface segregation for both the order and disorder phases by annealing the Cu_3Au crystal under UHV to reach an equilibrium state at 350°C and 500°C, respectively. Fig. 1(a) shows the XPS spectra of the Au 4f peaks obtained from the $Cu_3Au(100)$ annealed at 350°C with the incident photon energies of 400 eV and 1250 eV, respectively, where the surface segregation has reached a steady state, as confirmed by the saturated intensity of the Au 4f peaks with the longer annealing time.

The Au 4f region consists of two contributions corresponding to Au-$4f_{7/2}$ and Au-$4f_{5/2}$, respectively. Both contributions can be deconvoluted into two components, i.e., the bulk (B) and surface (S) components separated by surface core level shift[33]. The B and S component peaks are located at the binding energies of 84.5 eV and 84.0 eV for Au-$4f_{7/2}$ and 88.2 eV and 87.7 eV for Au-$4f_{5/2}$, respectively. These binding energies are consistent with previous reports on Cu-Au alloys[10,20,34,35]. The relative position of the B and S components is further confirmed by depth profiling using different photon energies. As shown in Fig. 1(a), the peak associated with the S component appears stronger with the smaller photon energy, and I_S/I_B peak area ratio increases from 0.23 to 0.89 as the photon energy increases from 1250 eV to 400 eV. This indicates that the S component is indeed more surface sensitive than the B component. The surface component can be referred to as pure Au because the surface segregation of Au results in the enrichment of Au atoms in the surface layer, giving it a higher probability of containing Au-Au bonds.

The bulk component corresponds to alloyed Au because the bulk has a lower concentration of Au atoms, giving it a higher probability of containing Au-Cu bonds.

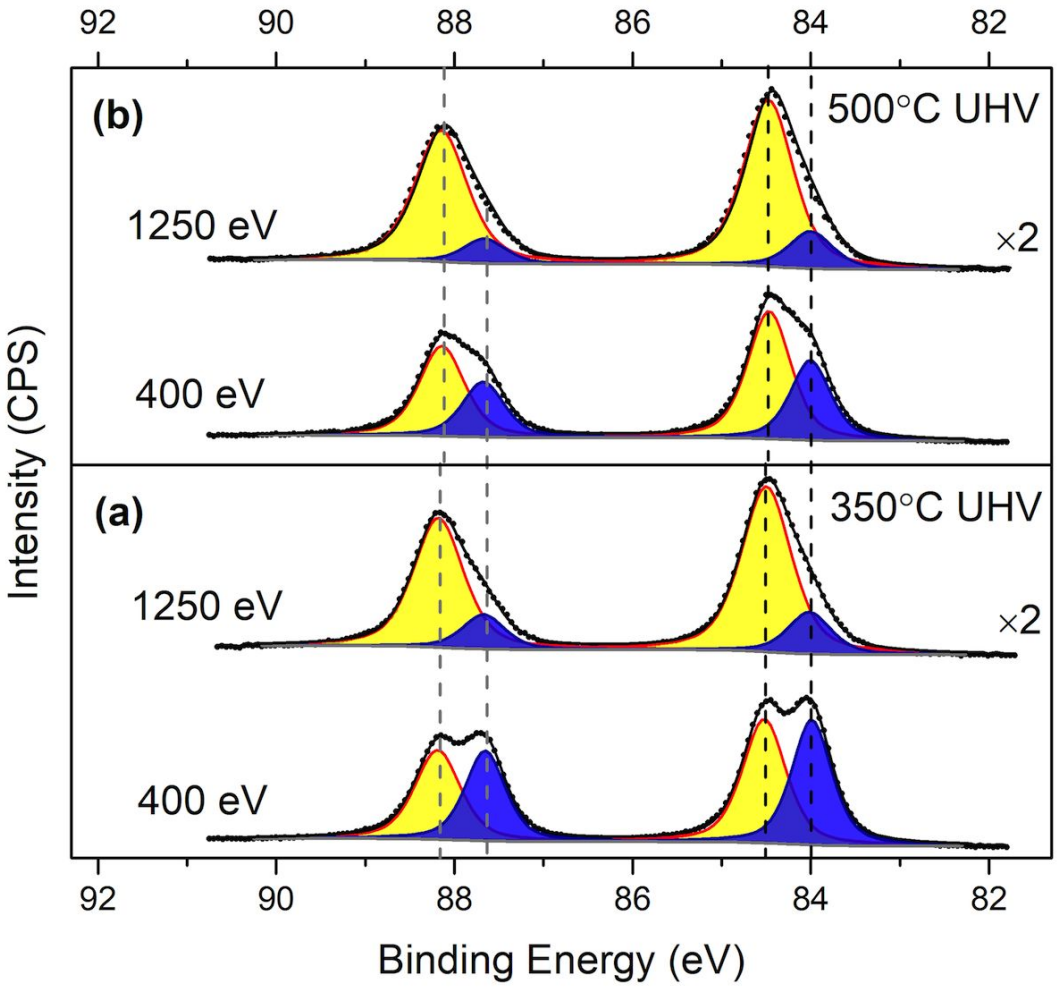

Figure 1: Au 4f region spectra of as-cleaned $Cu_3Au(100)$ under ultrahigh vacuum annealing, metallic Au (blue) and alloying Au (yellow) were observed for both ordered and disordered $Cu_3Au(100)$ at 350°C (a) and 500°C (b), respectively.

Fig. 1(b) corresponds to the Au 4f spectra obtained from the $Cu_3Au(100)$ at 500°C. Similarly, the Au surface segregation has reached a saturated state and the spectra can be deconvoluted into the B and S components, corresponding to alloyed Au in the bulk and pure Au in the surface, respectively. It can be noted that binding energy for the bulk component (alloyed Au) in the disorder phase shifts to a slightly lower binding energy by 0.1 eV compared to the alloyed Au in the order phase whereas the binding energy for the surface component (pure Au) remains the same for both the order and disorder phases[36].

Surprisingly, we find a weaker pure Au peak relative to the alloyed Au peak at 500°C. This is further confirmed by the smaller I_S/I_B peak area ratios of 0.29 and 0.65 at the photon energies of 1250 eV and 400 eV compared to those obtained from the Au surface segregation at 350°C in Fig. 1(b).

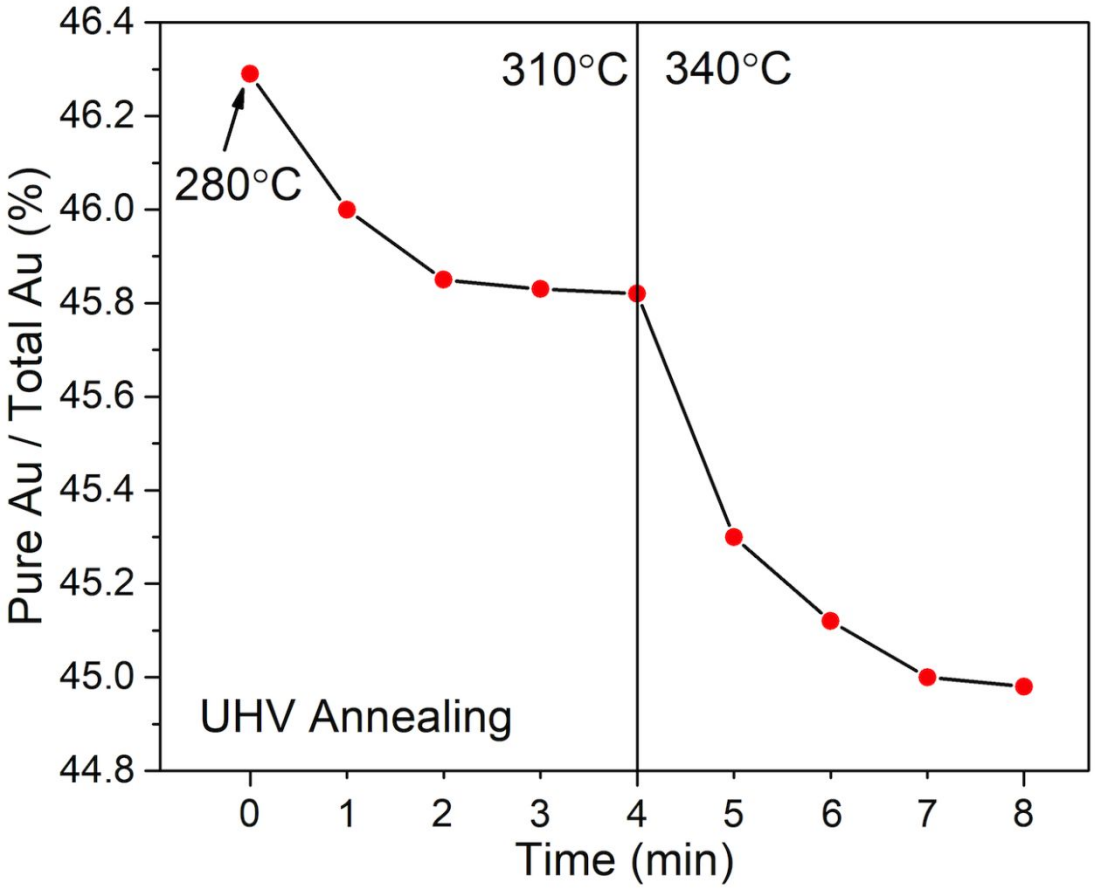

Figure 2: Temporal evolution of the pure Au component by quantifying the XPS spectra taken with the photon energy of 400 eV during the UHV annealing of the $Cu_3Au(100)$ crystal from 280°C to 340°C. The crystal was held isothermally at 340°C to allow for possible equilibration in surface composition.

The thickness of the segregated Au layer can be further estimated using a thin overlayer model. The thickness is given by[37] $t = -\lambda\, sin\theta \ln\left(1 + \frac{I_0/S_0}{I_s/S_s}\right)$, where λ is the inelastic free mean path, θ is the take-off angle with respect to the sample surface, I_0 and I_s are the peak area of the overlayer and substrate, S_0 and S_s are the scattering factors that are canceled out since both peaks are from the Au 4f region. The calculated thicknesses of the Au segregation layer are ~ 0.19 nm and 0.13 nm at 350°C and 500°C,

respectively, which correspond to ~ 0.9 monolayer (ML) and 0.6 ML of the surface coverage by pure Au on the (100) substrate (1 ML Au ~ 0.21 nm based on the FCC Au with the lattice parameter = 0.41 nm).

The evolution of the integrated peak area of the pure Au and alloyed Au components can be further quantified to determine the temporal changes of the surface composition under the UHV annealing. Fig. 2 illustrates the XPS measured pure Au content as a function of time as the sample is annealed from 280°C to 340°C, which shows that the pure Au component decreases with an increase in temperature. This trend is further confirmed by holding the sample at 340°C for possible equilibration, which shows that the surface Au approaches to a steady composition after ~ 4 min.

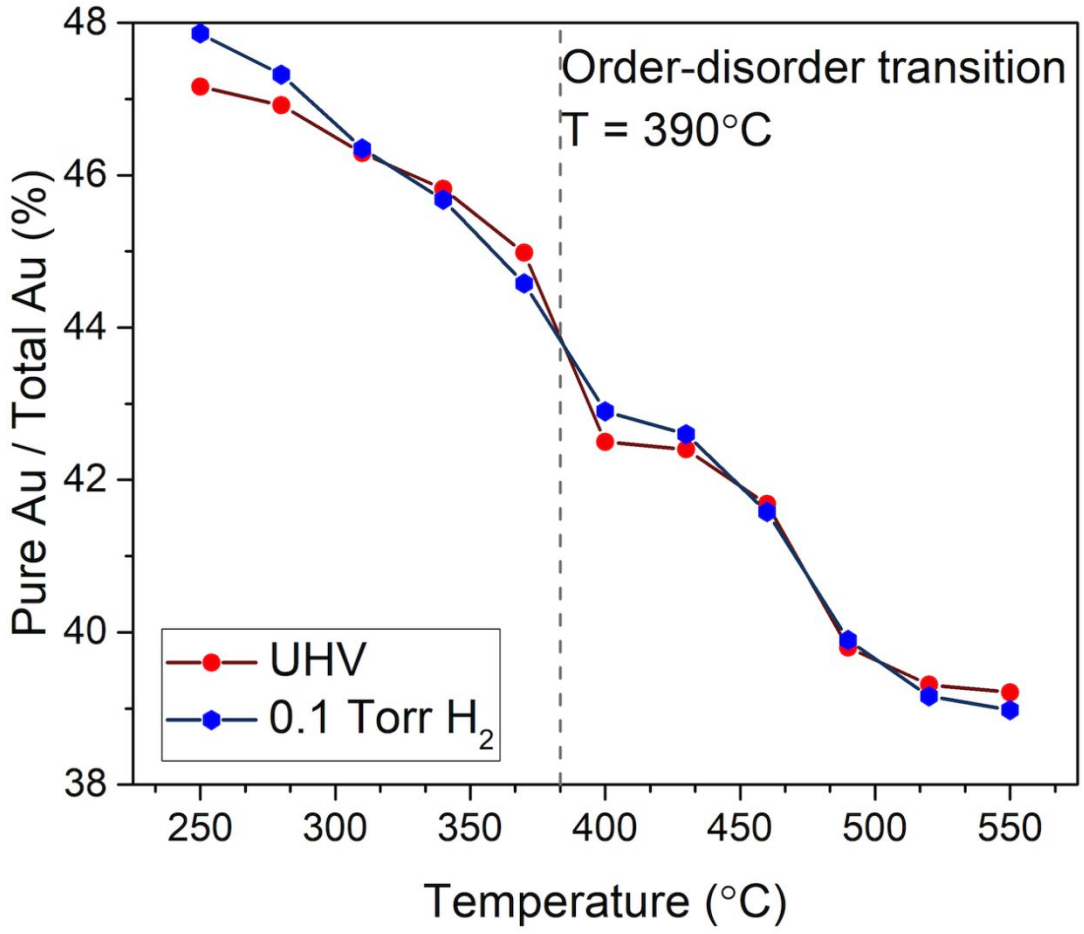

Figure 3: Comparison in surface metallic Au composition of $Cu_3Au(100)$ between UHV annealing and the annealing under the flow of H_2 gas at 0.1 Torr, spectra were taken with the photon energy of 400 eV. The annealing under the H_2 gas flow does not induce any notable differences in the surface Au content.

In addition to the UHV annealing shown above, we have also measured the surface composition evolution of the clean $Cu_3Au(100)$ surface during the annealing under the flow of H_2 gas at the pressure of 0.1 Torr. Fig. 3 illustrates the surface composition of metallic Au component obtained from the AP-XPS measurements of the clean $Cu_3Au(100)$ under the flow of H_2 gas. By comparing the UHV annealing at the different temperatures, no noticeable differences in the surface composition can be observed from the H_2 annealing. This is consistent with other studies showing the high dissociation barriers of H_2 molecules on both Cu and Au surfaces[38–40]. Even for atomic hydrogen, it bonds weakly to Cu and Au, and desorbs from Au surfaces at temperatures greater than ~ -163°C[41] and from Cu surfaces greater than ~80°C[42]. These measurements form the baseline to rule out any H_2 induced surface segregation in addition to its reaction with surface oxygen shown below.

3.2 Surface segregation of ordered Cu_3Au at 350°C and in reactive gases

The XPS measurements above demonstrate that Au segregates onto the surface under the vacuum annealing. This is driven by the lower surface energy of Au than Cu (γ_{Au} ~ 0.9 J/m^2, γ_{Cu} ~ 1.3 J/m^2). As shown below, this Au-terminated surface can be switched to the Cu-termination by oxygen adsorption. We first monitor the surface segregation behavior of ordered $Cu_3Au(100)$ upon its exposure to the flow of oxygen gas. The oxygen exposure induces the segregation of Cu atoms to the surface because the high oxygen affinity of Cu would more than compensate the unfavorable surface energy of Cu with respect to Au.

The freshly cleaned $Cu_3Au(100)$ is first annealed at 350°C under UHV to reach the saturated level of Au segregation (i.e., 0.9 ML surface coverage, as shown in Fig. 1). Fig. 4(a) illustrates the evolution of the Au 4f region upon the exposure of the well annealed $Cu_3Au(100)$ to $pO_2 = 1\times10^{-6}$ Torr at 350°C. It can be seen that there is a dramatic drop in the peak intensity of surface Au. After ~ 30 min of the oxygen exposure, the pure Au peak disappears completely. By contrast, the bulk component (alloyed Au) only has a slight increase in the peak intensity and its binding energy remains the same at 84 eV. This is evident from the temporal evolution of the integrated intensities of the pure Au and alloy peaks during

the O_2 dosing (Fig. 4(c)), which shows that the peak intensity for pure Au decays quickly while the peak intensity of alloyed Au only increases slightly and then quickly reaches a saturated level after 7 min of the oxygen exposure. The oxygen adsorption induced surface segregation of Cu requires efficient exchanges of Au atoms at the surface with Cu atoms in the subsurface. The relatively constant intensity of the alloyed Au peak along with the fast decay of the pure Au peak indicates that Au does not accumulate in the sub-surface but instead travels further deep into the bulk to form Cu-Au bonds. This also confirms the large atom mobility and the equilibrium segregation behavior shown above.

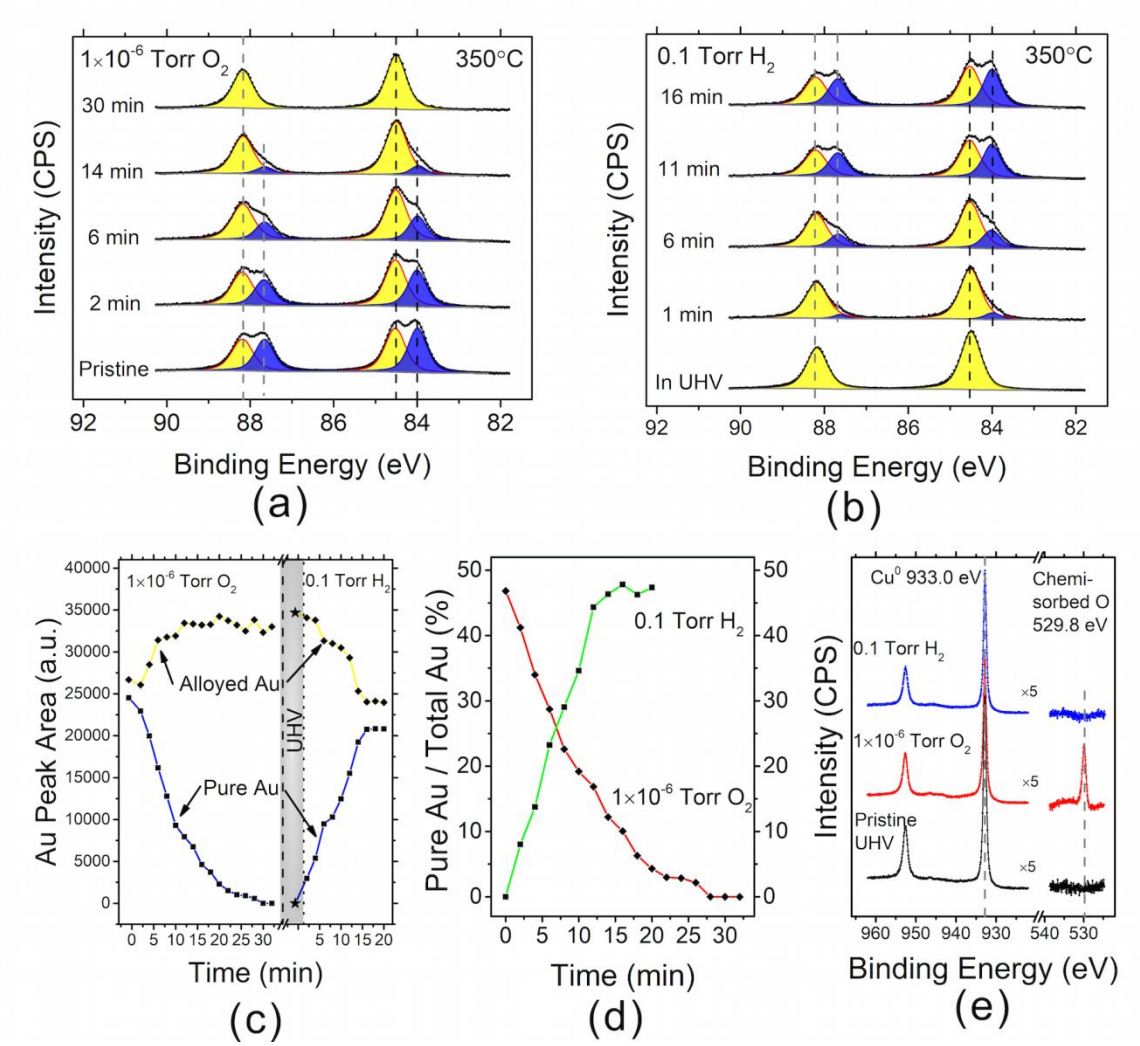

Figure 4: (a) Temporal evolution of the Au 4f spectra obtained from introducing chemisorbed O by dosing 1×10^{-5} Torr of O_2 gas at 350°C and (b) removing chemisorbed O by dosing 0.1 Torr of H_2 gas at 350°C. (c) Metallic Au (blue) and alloying Au (yellow) peak area and (d) metallic Au concentration changes during the gas dosing. (e) Cu 2p and O 1s spectra after the gas dosing confirming metallic state of Cu.

We then examine the stability of the oxygenated surface under UHV annealing and H_2 gas. Fig. 4(b) illustrates the XPS spectra of the Au 4f region obtained from the $Cu_3Au(100)$, first under the UHV annealing and then exposed to 0.1 Torr of H_2 gas flow, both maintained at 350°C. During the UHV annealing, the alloyed Au peak has no noticeable changes in the peak position and shape. This indicates that the UHV annealing at 350°C does not induce desorption of chemisorbed oxygen and the surface is still terminated by Cu with chemisorbed oxygen. As shown in Fig. 4(b), the subsequent exposure to the H_2 flow results in appreciable peak intensity associated with pure Au while the alloyed peak remains unchanged in its position but with slightly decreased intensity. The reappearance of pure Au at the surface indicates the segregation of Au atoms to the surface, which is induced by the loss of surface oxygen via its reaction with hydrogen to form H_2O molecules that desorb spontaneously from the surface. This is also consistent with previous studies showing the spontaneous reaction of chemisorbed oxygen on the Cu (110) surface with gaseous hydrogen that results in the pristine surface[43,44]. Upon the hydrogen induced loss of chemisorbed oxygen from the surface, Au segregation becomes more favorable because of its smaller surface energy and larger atom size. As shown in Fig. 4(b), the intensity of the pure Au peak increases with time and reaches a saturated level after ~ 16 min of the continuous H_2 flow, suggesting the complete removal of chemisorbed oxygen from the surface. Therefore, the H_2 dosing reverts the oxygenated surface to its pristine state that is oxygen free with ~ 0.9 ML of surface coverage of segregated Au atoms, as confirmed by comparing the Au 4f spectra between the surface after 16 min of the H_2 gas flow (Fig. 4(b)) and the pristine surface before O_2 dosing (Fig. 4(a)), both of which show the similar I_S/I_B peak area ratio of the pure Au and alloyed Au components. It is worth mentioning that the overall XPS peak intensity in the H_2 gas flow (Fig. 4(b)) is lower than that under the UHV annealing and O_2 flow as shown in Fig. 4(a). This is because of the scattering of the photoelectrons by gas molecules at the much higher pressure (0.1 Torr), which results in the attenuated peak intensity.

The surface composition evolution of the $Cu_3Au(100)$ under the O_2 and H_2 atmospheres is further evident by monitoring the peak intensity evolution of the pure Au and alloyed Au components. As shown in Fig. 4(c), the intensity for the pure Au peak drops to zero after ~ 30 min of the O_2 flow. By contrast, the

intensity for alloyed Au shows initially a slight increase and then remains constant, indicative of the slight enrichment of alloyed Au in the subsurface region. This is because of the oxygen adsorption induced surface segregation of Cu atoms that is in tandem with the inward flow of surface Au to the subsurface region. After the atmosphere is switched to the H_2 flow, the intensity associated with the pure Au component increases rapidly along with the drop of the alloyed Au to their saturated levels, indicating the surface segregation of Au from the subsurface region along with the inward diffusion of surface Cu to the subsurface region. As shown from such time-resolved XPS measurements, the coordinated evolution of the peak intensities of the pure Au and alloyed Au components demonstrates that the surface composition is quite sensitive to changes in the atmosphere and the segregation of the active component (either Au or Cu, depending on the atmosphere) occurs through the exchanges of atoms in the surface and subsurface. The integrated peak areas shown in Fig. 4(c) can be used to determine the evolution of pure Au with respect to the total Au (pure Au and alloyed Au) detected by the XPS measurements, as illustrated in Fig. 4(d). It can be noted from Fig. 4(d) that it takes ~ 30 min for converting the pure Au to alloyed Au in the O_2 atmosphere but only ~ 15 min to recover the pure Au at the surface in the H_2 atmosphere. This difference can be partly attributed to the different kinetic hurdles for the diffusion of Au atoms from and to the surface, where the migration of Au atoms from the surface to the subsurface (in the O_2 atmosphere) can be slower than that from the subsurface to the surface (in the H_2 atmosphere) because of the larger size of Au atoms as compared to Cu.

Chemical processes also happen at the surface upon the dosing of O_2 and H_2 gases. For instance, in the O_2 atmosphere, O_2 molecules need to dissociate into atomic O species. In the H_2 atmosphere, H_2 molecules dissociate into atomic H, and then react with O to make OH, and then H_2O before H_2O desorbs. It is known that molecular oxygen bonds weakly with Au surfaces with dissociation barriers larger than 1 eV[41]. As shown above, Au atoms segregate onto the $Cu_3Au(100)$ surface during UHV annealing. Therefore, the $Cu_3Au(100)$ surface is initially Au rich and oxygen adsorption by the Au-rich surface is thus slow during the O_2 exposure. This is also consistent with recent *in-situ* transmission electron microscopy observations, showing that a prolonged O_2 exposure is required to transform the Au-rich

surface of a Cu(Au) solid solution to an oxygenated surface with the resultant Cu-O surface termination[5]. By contrast, dissociative adsorption of H_2 molecules takes place easily on the oxygenated Cu surfaces[45], as also confirmed experimentally by monitoring the reaction of gaseous hydrogen with chemisorbed oxygen on Cu(110)[43,44]. Hence, the difference of dissociation rate of O_2 and H_2 on the Au-rich and oxygenated $Cu_3Au(100)$ surfaces may also contribute to the difference in the period of time required to revert the surface composition in the O_2 and H_2 atmospheres, respectively.

The chemical state of the $Cu_3Au(100)$ surface is also monitored in addition to the Au 4f spectra. As shown in Fig. 4(e), the shape and position of the Cu 2p core level peaks (binding energies = 932.9 eV and 952.5 eV) remain all the same for the pristine surface under the UHV annealing and in the flow of O_2 and H_2 gases, indicating that Cu remains as the metallic state and is not oxidized even in the O_2 atmosphere. This is because the low oxygen pressure (1×10^{-6} Torr) is adequate to drive the surface segregation of Cu atoms via oxygen chemisorption but not sufficient to result in Cu oxide formation. This is also in line with the previous study, showing that the crossover from oxygen chemisorption to Cu_2O formation requires a significantly higher oxygen pressure (~1×10^{-2} Torr) during the oxidation of Cu(100) at 350°C[46]. In our experiments, the surface uptake of chemisorbed oxygen during the O_2 exposure is also confirmed by the appreciable intensity in the O 1s region, as shown in Fig. 4(e). In the same way, the complete loss of chemisorbed oxygen from the hydrogen exposure is also confirmed by the absence of the O 1s peak intensity in Fig. 4(e).

3.3 Surface segregation of disordered Cu_3Au at 500°C and in reactive gases

We then monitor the surface segregation in disordered Cu_3Au by annealing the crystal at 500°C. The pristine surface shows ~ 0.6 ML coverage of pure Au under the UHV annealing (see Fig. 1). As shown in Fig. 5(a), the exposure to $pO_2 = 1\times10^{-6}$ Torr at 500°C results in fast decay of the peak intensity associated with the pure Au component along with a slight increase in the intensity of the alloyed Au component. The pure Au peak disappears completely after only ~ 5 min of the oxygen exposure, which is much faster than that (~ 30 min) for the oxygen dosing at 350°C. Fig. 5(b) shows the evolution of the Au

4f spectra after the chamber is first evacuated to UHV and then filled with the flow of H_2 gas at 0.1 Torr. The pure Au peak appears in the UHV annealing and quickly reaches a saturated level with the I_S/I_B area ratio similar as the pristine surface at 500°C, indicating that the chemisorbed oxygen is unstable and shows fast desorption from the surface under the UHV annealing. This is different from the ordered alloy at 350°C, where the UHV annealing does not induce oxygen desorption (Fig. 4(b)). As shown in Fig. 5(b), the subsequent H_2 dosing does not induce any noticeable changes to the Au 4f spectra in both the binding energy and the relative I_S/I_B peak area ratio, further confirming that the surface has reached an equilibrium concentration despite of the H_2 dosing.

Fig. 5(c) shows the temporal evolution of the integrated peak intensity of the pure Au and alloyed Au components in the O_2 and H_2 atmospheres, respectively. During the O_2 dosing, the peak intensity for the pure Au component quickly drops to zero along with coordinated increase of the peak intensity of the alloyed Au component. This indicates the oxygen adsorption induced Cu segregation from the subsurface region, which correspondingly results in the slight enrichment of alloyed Au in the subsurface region because of the inward migration of surface Au into the subsurface region. After switching to the UHV annealing, the pure Au peak intensity increases quickly due to the surface segregation of Au from the subsurface. The pure Au and alloyed peak intensities remain relatively unchanged in the subsequent H_2 flow, indicating that the equilibrium Au surface segregation has already reached under the UHV annealing. Similarly, the integrated peak intensities in Fig. 5(c) can be used to estimate the evolution of pure Au with respect to the total Au detected by the XPS measurements. As shown in Fig. 5(d), it takes ~ 6 min to convert the pure Au to alloyed Au in the O_2 atmosphere but it is almost instant to recover to the pure Au level at the surface after switching to UHV. This is because of the faster migration rate of Au atoms from the subsurface to the surface than the diffusion in the opposite direction. The $Cu_3Au(100)$ surface evolves much faster at 500°C to the equilibrium composition compared to the segregation at 350°C (Fig. 4(d)), in response to the changes in the atmosphere.

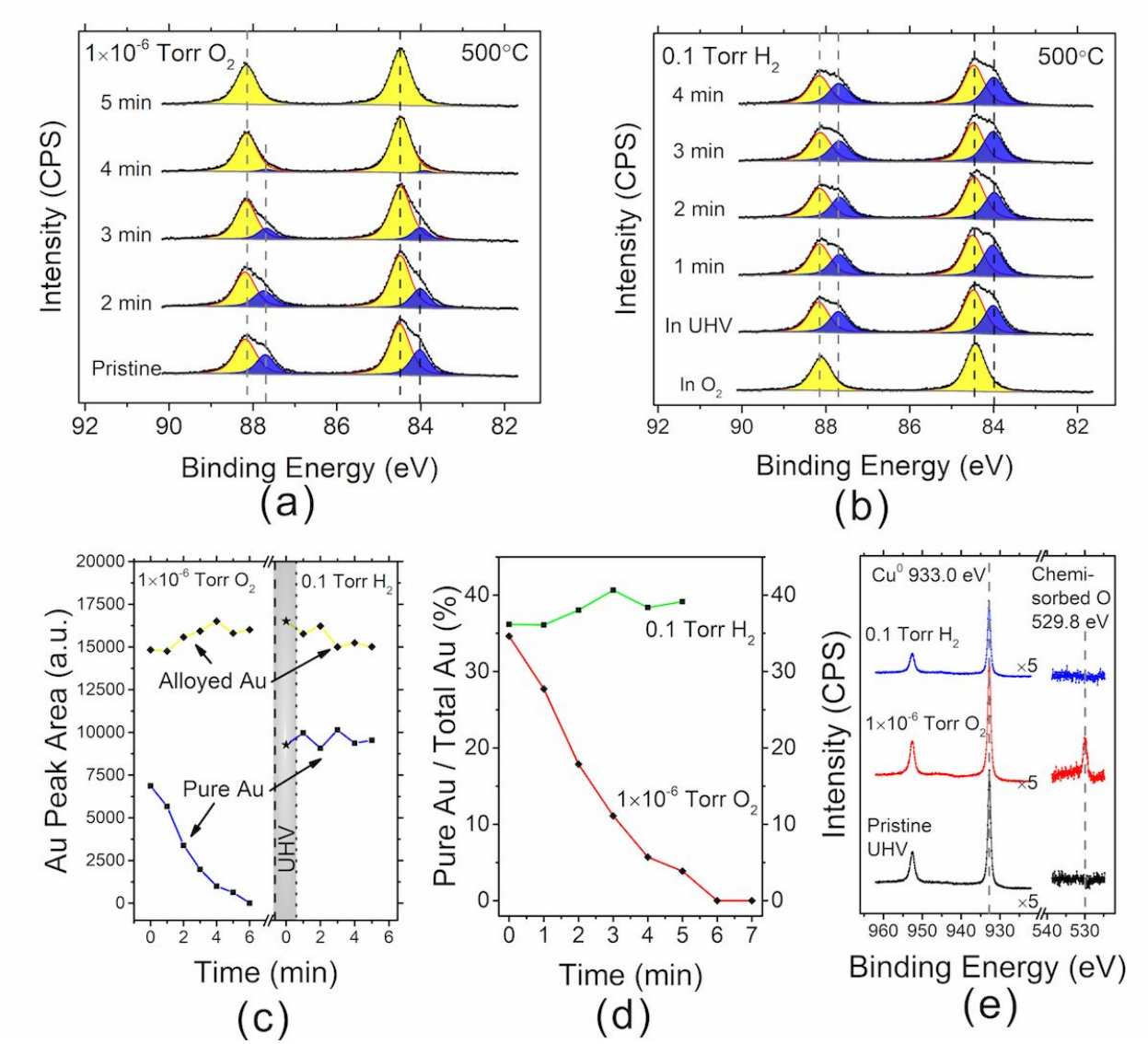

Figure 5: (a) Temporal evolution of the Au 4f spectra obtained from introducing chemisorbed O by dosing 1×10^{-5} Torr of O_2 gas at 500°C and (b) resuming the surface by dosing 0.1 Torr of H_2 gas at 500°C. (c) Metallic Au (blue) and alloying Au (yellow) peak area and (d) metallic Au concentration changes during the gas dosing. (e) Cu 2p and O 1s spectra after the gas dosing confirming metallic state of Cu.

Fig. 5(e) shows the chemical state of Cu and O under the UHV annealing and in the O_2 and H_2 atmospheres. The Cu 2p spectra show no noticeable changes in the flow of O_2 and H_2 gases from the pristine surface under the UHV annealing, indicating that Cu remains as the metallic state at the low oxygen pressure. The oxygen adsorption induced Cu segregation is confirmed by the appreciable intensity of O 1s spectra obtained during the O_2 exposure. Similarly, the re-segregation of pure Au to the surface

by the loss of chemisorbed oxygen in the H_2 atmosphere is also confirmed by the absence of the O 1s spectra.

3.4 Surface segregation in a highly oxidizing atmosphere

The measurements shown above demonstrate that the Au segregated surface under the UHV annealing can be tuned to the Cu termination with chemisorbed oxygen at low pO_2 (~1×10^{-6} Torr). Further increase in pO_2 would result in the formation of Cu oxides and we monitor the surface composition evolution in such a highly oxidizing atmosphere. As shown in Fig. 6(a), the oxygen exposure at pO_2 = 1 Torr and 350°C results in the complete attenuation of the Au 4f peak with the photon energy of 400 eV. Depth profiling with the higher photon energies of 700 eV and 1250 eV results in slight intensity in the Au 4f region but the peak positions are still not well resolved, indicating that the $Cu_3Au(100)$ is oxidized into a relatively thick layer of the Cu oxides. This is further confirmed with the O 1s spectra obtained from the oxidized surface. As shown in Fig. 6(b), the O 1s spectra can be deconvoluted into the two components with the binding energies of 529.5 eV and 530.2 eV corresponding to bulk CuO and surface CuO, respectively. The surface CuO component has a higher binding energy because of its lower coordination at the surface[47,48]. The surface and bulk components of the CuO layer are evident from the depth profiling with the different photon energies. As illustrated in Fig. 6(b), the peak associated with the surface CuO component becomes stronger as the photon energy decreases from 1250 eV to 700 eV, confirming that the higher binding component is more surface sensitive. Previous work[49] showed that Cu(100) can be oxidized to a CuO/Cu_2O bilayer structure under the condition of pO_2 = 1 Torr and 350°C. The oxygen in Cu_2O has the binding energy of 530.4 eV and is not detected here, suggesting that the thickness of the CuO layer is larger than the probe depth by the XPS. However, the existence of an inner Cu_2O layer is revealed from the XPS measurements by switching to the reducing atmosphere, as described below.

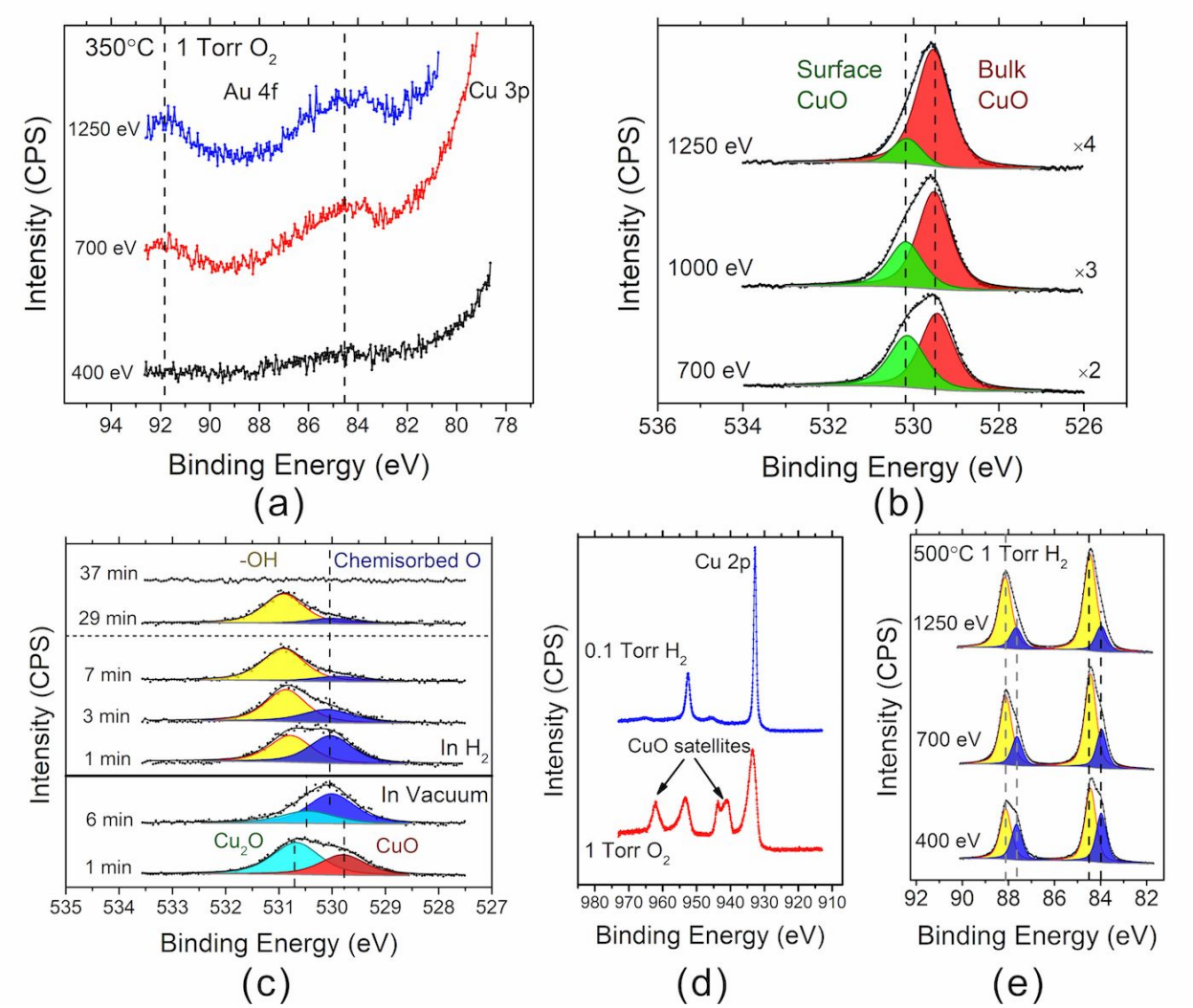

Figure 6: Au 4f (a) and O 1s (b) spectra measured at various photon energies after the oxidation of the $Cu_3Au(100)$ at 350°C with 1 Torr of O_2 gas flow. (c) O 1s peak evolution during the reduction at 500°C first under UHV, then in H_2, taken with 650 eV photon energy. (d) Cu 2p spectra confirming that Cu is oxidized to CuO at 350°C in the presence of 1 Torr of O_2 gas and is then reduced to metallic Cu at 500°C with 1 Torr of H_2 gas flow. (c) Metallic Au (blue) and alloying Au (yellow) measured at various photon energies after the reduction treatment at 500°C and 1 Torr of H_2 gas flow.

Fig. 6(c) shows the temporal evolution of the O 1s spectra when the oxidized $Cu_3Au(100)$ surface above is reduced at 500°C, first under UHV and then in the H_2 flow of 0.1 Torr. Under the UHV annealing, the CuO layer is unstable and already starts to decompose into Cu_2O. After 6 min of the UHV annealing, the CuO is completely reduced to Cu_2O with the presence of chemisorbed oxygen at the surface. After switching to 0.1 Torr of H_2 flow, the Cu_2O phase is quickly reduced, and only chemisorbed

O and OH are detectable, where the binding energy for OH shows small changes from 530.5 eV to 530.8 eV. This is probably due to the dynamic changes in the surface coverage of OH groups formed by the reaction between chemisorbed O and adsorbed H. The subsequent recombination reaction of OH groups with adsorbed H results in the formation of H_2O molecules that desorb spontaneously from the surface, as shown in a previous study[46]. After ~ 37 min of the H_2 flow, surface oxygen desorbs completely from the surface, as evidenced by the absence of peak intensity in the O 1s region in Fig. 6(c).

The surface oxidation and reduction is also monitored using the Cu 2p spectra. As shown in Fig. 6(d), the XPS spectra of the oxidized $Cu_3Au(100)$ surface display the Cu $2p_{3/2}$ and Cu $2p_{1/2}$ peaks together with a series of strong shakeup satellites that are the "fingerprint" of cupric ions in CuO. These satellites disappear with the long exposure to the H_2 gas flow, further confirming that the surface oxide is reduced. Fig. 6(e) shows the Au 4f spectra after the surface is recovered to its pristine state from the H_2 exposure. As illustrated by the depth profiling using the different photon energies, pure Au and alloyed Au peaks are visible and the pure Au peak is more surface-sensitive. Based on the peak intensity ratio of the two peaks, the pure Au has a surface coverage of ~ 0.6 ML, same as the pristine surface shown in Figs. 1(b) and 5(b). These measurements demonstrate that the surface composition evolution is highly reversible and tunable by controlling the atmosphere. However, it should be noted that it takes much longer time for the heavily oxidized surface to return to its pristine state in the H_2 atmosphere.

4. Discussion

Cu-Au has been extensively studied both experimentally and theoretically as a model system for understanding surface segregation phenomena in metal-based alloys[15,17,31,50–55]. Experimental studies on the surface layer composition profile of the Cu-Au alloys include AES[56–58], LEIS[31,59,60], medium-energy ion scattering[61], low-energy electron diffraction[60], and X-ray crystal truncation rod diffraction[50,54]. All these experimental studies were limited to clean surfaces under UHV and have showed that Au would enrich the surface. However, the resulting profound understanding obtained under the rarefied conditions does not translate into an equally good understanding of surface phenomena occurring in a

technologically relevant atmosphere, where the adsorption induced segregation can differ dramatically from the idealized conditions. Several XPS studies[9,20,34,62] using the "quench-and-look" approach by O_2 dosing followed by subsequent transfer to UHV for analysis have shown the inversion in surface composition from Au enrichment for a clean surface to Cu enrichment upon oxygen adsorption. Our AP-XPS results described above are not only in line with the previous studies but also provide important kinetic information of the adsorbate-induced surface segregation from the *in-situ* measurements under the flowing gas conditions. For instance, the detailed measurements of the temporal evolution of the surface compositions show a dynamic interplay between pure Au and alloying Au components before reaching a steady state of the surface composition. Such dynamic information is needed in order to tune the surface composition by utilizing competing actions of the environmental stimuli (UHV, O_2, H_2 and temperature) to control the degree of the surface segregation of an alloy component.

Gaining such a control over the surface segregation has important implications in tuning the surface reactivity of alloys that are widely used for heterogeneous catalytic processes. The catalytic performance is intimately related to the oxidation of the alloy surfaces. The presence of surface and interface oxygen on alloy catalysts must be considered because such species are present in the majority of real-world catalysts under reaction conditions. Their role in catalysis is still very unclear and need to be investigated on a case-by-case basis. The catalytic reactions on some alloys actually occur due to the surface oxidation. Recent studies on catalytic oxidation of CO and H_2 have suggested that the presence of a surface (or interface) oxide can make the catalyst catalytically more reactive than the corresponding pristine alloy surfaces[63,64]. A microscopic understanding of such a synergistic catalytic effect requires atomic-level knowledge of the adsorbate-induced elemental segregation process taking place on the outer surface layers of alloy catalysts during the catalytic reactions. As shown from our AP-XPS measurements of the surface segregation on $Cu_3Au(100)$, the surface composition of the alloy does not stay stationary over time, even under the UHV condition. Instead, it shows dynamic changes in response to the external stimuli, which can lead to numerous surface configurations over the segregation process. These results

provide the baseline for manipulating the environmental conditions to affect the reaction kinetics and mechanism.

5. Conclusion

In conclusion, we have studied how the surface composition of the binary $Cu_3Au(100)$ can be tuned via its response to the atmosphere. Under the UHV annealing, Au segregation to the pristine surface results in pure Au at the surface and alloyed Au in the subsurface, and the amount of pure Au decreases with increasing the annealing temperature. Upon the exposure to an oxidizing atmosphere, the Au terminated surface transforms to a Cu-O terminated surface driven by oxygen-adsorption induced Cu segregation. It is further demonstrated that the Cu terminated surface can revert to the Au termination by switching to UHV annealing or a H_2 atmosphere that results in the surface desorption of oxygen, thereby promoting Au segregation to the surface. The results reported here may serve as a guide for the choice of optimal environmental conditions to tune the surface composition of alloys, which has practical implications for controlling the surface properties such as catalytic performance and corrosion resistance.

Acknowledgements

This work was supported by the U.S. Department of Energy, Office of Basic Energy Sciences, Division of Materials Sciences and Engineering under Award No. DE-SC0001135. This research used resources of the 23-ID-2 (IOS) beamline at the National Synchrotron Light Source II and the Center for Functional Nanomaterials, which are U.S. DOE Office of Science Facilities, at Brookhaven National Laboratory under Contract No. DE-SC0012704.

Reference

1 I. Zegkinoglou, L. Pielsticker, Z.-K. Han, N. J. Divins, D. Kordus, Y.-T. Chen, C. Escudero, V. Pérez-Dieste, B. Zhu, Y. Gao and B. R. Cuenya, Surface Segregation in CuNi Nanoparticle Catalysts During CO_2 Hydrogenation: The Role of CO in the Reactant Mixture, *J. Phys. Chem. C*, 2019, **123**, 8421–8428.

2 J. P. Simonovis, A. Hunt, R. M. Palomino, S. D. Senanayake and I. Waluyo, Enhanced Stability of Pt-Cu Single-Atom Alloy Catalysts: In Situ Characterization of the Pt/Cu (111) Surface in an Ambient Pressure of CO, *J. Phys. Chem. C*, 2018, **122**, 4488–4495.

3 Y. Iguchi, G. L. Katona, C. Cserháti, G. A. Langer and Z. Erdélyi, On the miscibility gap of Cu-Ni system, *Acta Mater.*, 2018, **148**, 49–54.

4 S.-H. Ha, B.-H. Kim, Y.-O. Yoon, H.-K. Lim, D.-H. Kim and S. K. Kim, Surface Enrichment of Mg and Ca in Cu–Mg Alloy Containing a Trace Amount of Ca and Its Effects on Oxidation Resistance, *J. Nanosci. Nanotechnol.*, 2019, **19**, 1734–1737.

5 L. Zou, W. A. Saidi, Y. Lei, Z. Liu, J. Li, L. Li, Q. Zhu, D. Zakharov, E. A. Stach, J. C. Yang, G. Wang and G. Zhou, Segregation induced order-disorder transition in Cu(Au) surface alloys, *Acta Mater.*, 2018, **154**, 220–227.

6 L. Zou, C. Yang, Y. Lei, D. Zakharov, J. M. K. Wiezorek, D. Su, Q. Yin, J. Li, Z. Liu, E. A. Stach, J. C. Yang, L. Qi, G. Wang and G. Zhou, Dislocation nucleation facilitated by atomic segregation, *Nat. Mater.*, 2017, **17**, 56.

7 J. Y. Zhang, J. T. Zhao, X. G. Li, Y. Q. Wang, K. Wu, G. Liu and J. Sun, Alloying effects on the microstructure and mechanical properties of nanocrystalline Cu-based alloyed thin films: Miscible Cu-Ti vs immiscible Cu-Mo, *Acta Mater.*, 2018, **143**, 55–66.

8 J. B. Seol, D. Haley, D. T. Hoelzer and J. H. Kim, Influences of interstitial and extrusion temperature on grain boundary segregation, Y−Ti−O nanofeatures, and mechanical properties of ferritic steels, *Acta Mater.*, 2018, **153**, 71–85.

9 E. Völker, F. J. Williams, E. J. Calvo, T. Jacob and D. J. Schiffrin, O2 induced Cu surface

segregation in Au–Cu alloys studied by angle resolved XPS and DFT modelling, *Phys. Chem. Chem. Phys.*, 2012, **14**, 7448–7455.

10 Y. Tsuda, K. Oka, T. Makino, M. Okada, W. A. Diño, M. Hashinokuchi, A. Yoshigoe, Y. Teraoka and H. Kasai, Initial stages of $Cu_3Au(111)$ oxidation: oxygen induced Cu segregation and the protective Au layer profile, *Phys. Chem. Chem. Phys.*, 2014, **16**, 3815–3822.

11 M. Polak and L. Rubinovich, The interplay of surface segregation and atomic order in alloys, *Surf. Sci. Rep.*, 2000, **38**, 127–194.

12 A. V Ruban, H. L. Skriver and J. K. Nørskov, Surface segregation energies in transition-metal alloys, *Phys. Rev. B*, 1999, **59**, 15990–16000.

13 G. Wang, M. A. Van Hove, P. N. Ross and M. I. Baskes, Quantitative prediction of surface segregation in bimetallic Pt–M alloy nanoparticles (M= Ni, Re, Mo), *Prog. Surf. Sci.*, 2005, **79**, 28–45.

14 H. Okamoto, D. J. Chakrabarti, D. E. Laughlin and T. B. Massalski, The Au−Cu (Gold-Copper) system, *J. Phase Equilibria*, 1987, **8**, 454.

15 K. R. Mecke and S. Dietrich, Segregation profiles in Cu_3Au above the order-disorder transition, *Phys. Rev. B*, 1995, **52**, 2107–2116.

16 J. R. Chelikowsky, Predictions for surface segregation in intermetallic alloys, *Surf. Sci.*, 1984, **139**, L197–L203.

17 J. M. Sanchez and J. L. Moran-López, Ordering and segregation at (001) surfaces of Cu_3Au, *Surf. Sci.*, 1985, **157**, L297–L302.

18 G. W. Graham, Oxygen adsorption on $Cu_3Au(100)$ above 350 K, *Surf. Sci.*, 1984, **137**, L79–L83.

19 K. J. Andersson, F. Calle-Vallejo, J. Rossmeisl and I. Chorkendorff, Adsorption-Driven Surface Segregation of the Less Reactive Alloy Component, *J. Am. Chem. Soc.*, 2009, **131**, 2404–2407.

20 M. Okada, Y. Tsuda, K. Oka, K. Kojima, W. A. Diño, A. Yoshigoe and H. Kasai, Experimental and Theoretical Studies on Oxidation of Cu-Au Alloy Surfaces: Effect of Bulk Au Concentration, *Sci. Rep.*, 2016, **6**, 31101.

21 S. Zafeiratos, S. Piccinin and D. Teschner, Alloys in catalysis: phase separation and surface segregation phenomena in response to the reactive environment, *Catal. Sci. Technol.*, 2012, **2**, 1787–1801.

22 Y. Ma and P. B. Balbuena, Surface segregation in bimetallic Pt3M (M= Fe, Co, Ni) alloys with adsorbed oxygen, *Surf. Sci.*, 2009, **603**, 349–353.

23 J. R. Kitchin, K. Reuter and M. Scheffler, Alloy surface segregation in reactive environments: first-principles atomistic thermodynamics study of Ag_3Pd (111) in oxygen atmospheres, *Phys. Rev. B*, 2008, **77**, 75437.

24 B. C. Han, A. Van der Ven, G. Ceder and B.-J. Hwang, Surface segregation and ordering of alloy surfaces in the presence of adsorbates, *Phys. Rev. B*, 2005, **72**, 205409.

25 H. Niehus and C. Achete, Surface structure investigation of nitrogen and oxygen on $Cu_3Au(100)$, *Surf. Sci.*, 1993, **289**, 19–29.

26 D. E. Starr, Z. Liu, M. Hävecker, A. Knop-Gericke and H. Bluhm, Investigation of solid/vapor interfaces using ambient pressure X-ray photoelectron spectroscopy, *Chem. Soc. Rev.*, 2013, **42**, 5833–5857.

27 L. Zou, J. Li, D. Zakharov, W. A. Saidi, E. A. Stach and G. Zhou, Atomically Visualizing Elemental Segregation-Induced Surface Alloying and Restructuring, *J. Phys. Chem. Lett.*, 2017, **8**, 6035–6040.

28 V. Kumar and K. H. Bennemann, Order-Disorder Transitions and Segregation at the (100) Surface of Cu-Au Alloys, *Phys. Rev. Lett.*, 1984, **53**, 278.

29 S. Hüfner, *Photoelectron spectroscopy: principles and applications*, Springer Science & Business Media, 2013.

30 J. C. Vickerman and I. S. Gilmore, *Surface analysis: the principal techniques*, John Wiley & Sons, 2011.

31 T. M. Buck, G. H. Wheatley and L. Marchut, Order-Disorder and Segregation Behavior at the $Cu_3Au(001)$ Surface, *Phys. Rev. Lett.*, 1983, **51**, 43–46.

32 J. Li, G. Wang and G. Zhou, Surface segregation phenomena in extended and nanoparticle surfaces of Cu–Au alloys, *Surf. Sci.*, 2016, **649**, 39–45.

33 P. Heimann, J. F. Van Der Veen, D. E. Eastman and Y. Heights, ~Solid State Communications, Voi.38, *Solid State Commun.*, 1981, **38**, 595–598.

34 K. Oka, Y. Tsuda, T. Makino, M. Okada, M. Hashinokuchi, A. Yoshigoe, Y. Teraoka and H. Kasai, The effects of alloying and segregation for the reactivity and diffusion of oxygen on $Cu_3Au(111)$, *Phys. Chem. Chem. Phys.*, 2014, **16**, 19702–19711.

35 S. B. DiCenzo, P. H. Citrin, E. H. Hartford and G. K. Wertheim, Au surface density of states and surface core-level shifts in $Cu_3Au(001)$, *Phys. Rev. B*, 1986, **34**, 1343–1345.

36 M. Kuhn and T. K. Sham, Charge redistribution and electronic behavior in a series of Au-Cu alloys, *Phys. Rev. B*, 1994, **49**, 1647–1661.

37 M. P. Seah and D. Briggs, *Practical Surface Analysis: Auger and X-ray Photoelectron Spectroscopy*, John Wiley & Sons, 1990.

38 B. Hammer and J. K. Norskov, Why gold is the noblest of all the metals, *Nature*, 1995, **376**, 238–240.

39 L. Stobiński and R. Duś, Model of atomic hydrogen adsorption on thin gold film surface, *Vacuum*, 1994, **45**, 299–301.

40 J. Greeley and M. Mavrikakis, Surface and Subsurface Hydrogen: Adsorption Properties on Transition Metals and Near-Surface Alloys, *J. Phys. Chem. B*, 2005, **109**, 3460–3471.

41 M. Pan, A. J. Brush, Z. D. Pozun, H. C. Ham, W.-Y. Yu, G. Henkelman, G. S. Hwang and C. B. Mullins, Model studies of heterogeneous catalytic hydrogenation reactions with gold, *Chem. Soc. Rev.*, 2013, **42**, 5002–5013.

42 I. Yasumori, N. Momma and M. Kiyomiya, Mechanism of Hydrogen Adsorption and Hydrogen-Deuterium Equilibration on Copper Surface, *Jpn. J. Appl. Phys.*, 1974, **13**, 485.

43 W. Shan, Q. Liu, J. Li, N. Cai, W. A. Saidi and G. Zhou, Hydrogen-induced atomic structure evolution of the oxygen-chemisorbed Cu(110) surface, *J. Chem. Phys.*, 2016, **145**, 234704.

44 Y. Zhu, D. Wu, Q. Liu, J. T. Sadowski and G. Zhou, Hydrogen-Induced Clustering of Metal Atoms in Oxygenated Metal Surfaces, *J. Phys. Chem. C*, 2019, **123**, 11662–11670.

45 G. Hao, R. Zhang, J. Li, B. Wang and Q. Zhao, Insight into the effect of surface structure on H2 adsorption and activation over different CuO(111) surfaces: A first-principle study, *Comput. Mater. Sci.*, 2016, **122**, 191–200.

46 J. Wang, C. Li, Y. Zhu, J. A. Boscoboinik and G. Zhou, Insight into the Phase Transformation Pathways of Copper Oxidation: From Oxygen Chemisorption on the Clean Surface to Multilayer Bulk Oxide Growth, *J. Phys. Chem. C*, 2018, **122**, 26519–26527.

47 W. F. Egelhoff, Core-level binding-energy shifts at surfaces and in solids, *Surf. Sci. Rep.*, 1987, **6**, 253–415.

48 S. L. Harmer, W. M. Skinner, A. N. Buckley and L.-J. Fan, Species formed at cuprite fracture surfaces; observation of O 1s surface core level shift, *Surf. Sci.*, 2009, **603**, 537–545.

49 L. Yuan, Y. Wang, R. Mema and G. Zhou, Driving force and growth mechanism for spontaneous oxide nanowire formation during the thermal oxidation of metals, *Acta Mater.*, 2011, **59**, 2491–2500.

50 H. Reichert, P. J. Eng, H. Dosch and I. K. Robinson, Thermodynamics of Surface Segregation Profiles at $Cu_3Au(001)$ Resolved by X-Ray Scattering, *Phys. Rev. Lett.*, 1995, **74**, 2006–2009.

51 S. M. Foiles, Ordered surface phases of Au on Cu, *Surf. Sci.*, 1987, **191**, 329–338.

52 M. Hou and M. El Azzaoui, A Monte Carlo study of the thermal properties of Cu_3Au low index surfaces, *Surf. Sci.*, 1997, **380**, 210–223.

53 M. Hayoun, V. Pontikis and C. Winter, Computer simulation study of surface segregation on Cu_3Au, *Surf. Sci.*, 1998, **398**, 125–133.

54 H. Reichert and H. Dosch, Surface segregation in Cu_3Au (001), *Surf. Sci.*, 1996, **345**, 27–40.

55 M. A. Hoffmann and P. Wynblatt, Surface composition of dilute copper-gold alloys, *Surf. Sci.*, 1990, **236**, 369–376.

56 S. Mróz, Composition of the first atomic layers of (001)-oriented $AuCu_3$ crystal measured with the

use of directional Auger electron spectroscopy at 400K<T<1000K, *Vacuum*, 2005, **79**, 241–249.

57 S. Mróz and A. Krupski, Composition of the first two atomic layers in $Au_{0.2}Cu_{0.8}$ and $Au_{0.8}Cu_{0.2}$ alloys, *Vacuum*, 2001, **60**, 307–313.

58 J. M. McDavid and S. C. Fain, Segregation at CuAu alloy surfaces, *Surf. Sci.*, 1975, **52**, 161–173.

59 M. J. Sparnaay and G. E. Thomas, Surface segregation in $Au_{0.1}Cu_{0.9}$ crystals, *Surf. Sci.*, 1983, **135**, 184–198.

60 E. G. McRae, T. M. Buck, R. A. Malic, W. E. Wallace and J. M. Sanchez, Ordering and layer composition at the $Cu_3Au(110)$ surface, *Surf. Sci.*, 1990, **238**, L481–L485.

61 D. H. Oh, H. J. Kang, K. H. Chae, C. N. Whang, B. V King, D. J. O'Connor and D. W. Moon, Compositional changes in the surface layers of the $Cu_3Au(100)$ below the bulk transition temperature, *Surf. Sci.*, 2001, **477**, L289–L294.

62 M. Okada, K. Moritani, T. Fukuyama, H. Mizutani, A. Yoshigoe, Y. Teraoka and T. Kasai, Comparative study of oxidation on Cu and Cu_3Au surfaces with a hyperthermal O_2 molecular beam, *Surf. Sci.*, 2006, **600**, 4228–4232.

63 H. Lee, J. Lim, C. Lee, S. Back, K. An, J. W. Shin, R. Ryoo, Y. Jung and J. Y. Park, Boosting hot electron flux and catalytic activity at metal–oxide interfaces of PtCo bimetallic nanoparticles, *Nat. Commun.*, 2018, **9**, 2235.

64 J. Kim, W. H. Park, W. H. Doh, S. W. Lee, M. C. Noh, J.-J. Gallet, F. Bournel, H. Kondoh, K. Mase, Y. Jung, B. S. Mun and J. Y. Park, Adsorbate-driven reactive interfacial Pt-NiO nanostructure formation on the PtNi(111) alloy surface, *Sci. Adv.*, 2018, **4**, eaat3151.